Spin-polarization spectroscopy of Auger electrons and photoelectrons in 5p ionization of barium atoms

R. Kuntze,[1] M. Salzmann,[1] N. Böwering,[1] U. Heinzmann,[1] V. K. Ivanov,[2] and N. M. Kabachnik[1,3]

[1] *Fakultät für Physik, Universität Bielefeld, 33501 Bielefeld, Federal Republic of Germany and Fritz-Haber-Institut der Max-Planck-Gesellschaft, 14195 Berlin, Federal Republic of Germany*

[2] *St. Petersburg Technical University, 195251 St. Petersburg, Russia*

[3] *Institute of Nuclear Physics, Moscow State University, Moscow 119899, Russia*

(Received 16 December 1993)

We report on experimental studies of the photon energy dependence of the Auger yield and the spin polarization of Auger electrons and photoelectrons after photoionization of the 5p subshell of free Ba atoms with circularly polarized light for photon energies between 22 and 31 eV. Relations between the dynamics of the Auger-decay and the photoelectron emission are derived and their validity is probed from the experimental results. Our data are compared with numerical calculations, which were performed in the Hartree-Fock and in the random-phase approximation with exchange approach.

PACS number(s): 32.80.Fb, 32.80.Hd, 31.20.Di

I. INTRODUCTION

Auger electrons emitted in the decay of an inner-shell vacancy may be spin polarized if the hole states created have a nonstatistical distribution of their magnetic sublevels. An alignment of the vacancies can arise even when unpolarized light or particles are used for ionization of an unpolarized target (for a review, see Mehlhorn [1, 2]). For this case, a so-called dynamical Auger-electron polarization occurring only in the direction perpendicular to the plane of reaction was predicted [3, 4] and subsequently observed [5, 6], although it was found to be small. The alignment, however, may influence the electron angular distribution considerably, as was observed for the rare gases Ar, Kr, and Xe [7]. If the incident light is circularly polarized, an efficient polarization transfer can take place leading to inner-shell vacancies with not only aligned but, moreover, oriented angular momenta. The polarization of the ionic states may then be partially passed to the outgoing Auger electrons generally giving rise to nonzero values for all three components of the spin-polarization vector of the Auger-electrons [3]. This case was discussed in detail theoretically [8] and recently observed experimentally for free barium atoms [9] and in the Auger-electron emission from rubidium adlayers [10] using circularly polarized synchroton radiation. In a previous paper on the Ba Auger-electron polarization [9] the angular distributions of the polarization component $A(\theta)$ were discussed. Furthermore, they were analyzed in order to extract directly from the experiment the orientation and the alignment coefficients of the intermediate excited ionic state as well as the ratio of the photoelectron transition matrix elements. The emphasis of the present paper is primarily on the investigation of the photon energy dependence of the spin polarization of the $5p^{-1}$-$6s^{-2}$ Auger electron doublet (equivalent notation: $O_{2,3}$-P_1P_1), and also of the corresponding photoelectrons, by both experimental and theoretical methods.

The creation of a 5p hole state in atomic Ba has been the subject of several experimental studies in the past. In the process investigated here an electron is removed from the 5p subshell by photoionization and the excited Ba^+ ion decays via emission of an Auger electron. This can be described as follows:

$$\mathrm{Ba}(5p^6 6s^2)\,{}^1S_0 + h\nu \rightarrow \mathrm{Ba}^+(5p^5 6s^2)\,{}^2P_J + e^-_{\mathrm{photo}}(\epsilon s, \epsilon d)$$
$$\downarrow$$
$$\mathrm{Ba}^{2+}(5p^6)\,{}^1S_0 + e^-_{\mathrm{Auger}}(\epsilon p_J).$$

Here, $J = 1/2, 3/2$ denotes the total angular momentum of the photoion state and the Auger electron. Above $h\nu \simeq 21$ eV this is the dominant process and fluorescence decay can be neglected, as was shown by measurements of the photon energy dependence of the Ba^{2+} to Ba^+ ratio [11]. High-resolution absorption spectra were recorded [12, 13] and a pronounced resonance structure was detected at photon energies between $h\nu \simeq 22$ eV and $h\nu \simeq 25$ eV, which is due to autoionization resonances, giving rise to complex absorption spectra. The resonances were found to be members of a Rydberg series converging to dominant lines of the absorption spectrum of Ba^+ [14]. The first Ba Auger-electron intensity measurements after 5p excitation were performed after the creation of the initial hole state by electron impact [15, 16]. Many Auger satellite lines were observed in these spectra and assignments of the intermediate states were given by Rassi and Ross [16]. Measurements of the photoelectron and Auger-electron intensity after photoionization with He I radiation [17] and with synchrotron radiation [18–20] have also been reported. The 5p photoabsorption in Ba was considered theoretically by Wendin [21] within the framework of random-phase approximation with exchange (RPAE) taking interacting $(5p; nd)^1P_1$ and $(6s; np)^1P_1$ channels into account. The

$5p$ alignment after photoionization was discussed previously by Berezhko *et al.* using a simple Herman-Skillman potential [22] and in the Hartree-Fock (HF) and RPAE approaches [23].

In the present work we report on measurements of the energy dependence of both intensity and spin polarization of the O_2-P_1P_1 and O_3-P_1P_1 Auger electron lines after photoionization of the $5p$ subshell with circularly polarized radiation. At several photon energies we measured also the corresponding photoelectron spin polarization containing information about the phase difference between the outgoing partial electron waves, in addition to the transition amplitudes. In contrast to the photoelectron case, the dynamical parameters of the Auger electron for a $^1S_0$ final ionic state examined here do not provide any phase information. Our experimental data are compared with dynamical parameters, determined in the framework of Kabachnik and Lee [8] from transition matrix elements of the photoelectrons calculated in the Hartree-Fock [23] and RPAE approaches. Related theoretical calculations of the Auger-electron polarization for noble gases [24, 25] and Hg [26] have been performed recently.

II. EXPERIMENT

For the ionization of the Ba atoms circularly polarized synchrotron radiation from the 6.5 m normal incidence monochromator (degree of circular polarization: 0.92 ± 0.03) at the Berlin electron storage ring BESSY was used [27]. For spin polarization as well as for intensity measurements an osmium coated grating with 3600 lines/mm was employed. It has a maximum transmission at $h\nu \simeq 21$ eV and a resolution of $\Delta\lambda = 0.18$ nm with a 2 mm wide exit slit and of $\Delta\lambda = 0.36$ nm with a 4 mm wide exit slit. The effusive barium atom beam was generated with a boron nitride oven, resistively heated to about 850 ° C. The temperature was measured with a pyrometer. To improve the collimation of the atomic beam a Laval nozzle was used with the exit hole at a distance of about 1 mm from the light focus. The photoelectrons and Auger electrons emitted in the magnetic-field-free ionization region were detected energy- and angle-resolved by means of a rotatable simulated hemispherical spectrometer [28, 29] which was operated with an electrostatic three-element entrance optics to increase its transmission. The deposition of barium at the spectrometer entrance slit lowered the transmission of electrons with $E_{\text{kin}} \leq 3$ eV seriously due to contact potentials. The electron spin polarization was measured by detecting $A(\theta)$, parallel to the photon beam, and $P_\perp(\theta)$, normal to the reaction plane, which is defined by the $\mathbf{k}$ vectors of the incident light and the outgoing electron [30]

$$A(\theta) = \gamma \frac{A - \alpha\, P_2(\cos\theta)}{1 - \frac{\beta}{2}\, P_2(\cos\theta)}, \tag{1}$$

$$P_\perp(\theta) = \frac{2\,\xi \sin\theta \cos\theta}{1 - \frac{\beta}{2}\, P_2(\cos\theta)}, \tag{2}$$

where θ is the angle between the incoming light and the outgoing electron. A, ξ, α, and β are dynamical parameters describing the photoionization process as well as the Auger-electron emission (see Sect. III). $P_2(\cos\theta)$ denotes the second Legendre polynomial and γ is the light helicity. According to Ref. [8] the equations for the angular dependence of the polarization components apply also for the case of Auger electrons. The validity of Eq. (1) was shown experimentally for photoelectrons in Ref. [30] and for Auger electrons in Ref. [9].

For the spin analysis a high-voltage Mott detector (100 kV, Sherman function: -0.23 ± 0.02) was used [29]. The count rate at the detectors in the Mott analyzer was typically only 1 Hz or less. In our experimental geometry, it is sufficient for the determination of the dynamical parameters A and ξ to measure the spin polarization at the positive and negative magic angles $\theta_{\text{mag}} = \pm 54.7°$ with alternating light helicity. For the additional determination of the spin-polarization asymmetry parameter α and the intensity asymmetry parameter β, the angular dependence of $A(\theta)$ has to be determined [9], which was done only at one particular photon energy.

III. THEORY

A general theory of the spin polarization of Auger electrons following photoionization with arbitrarily polarized light was worked out in the past [3, 8]. Using the developed formalism, the dynamical features can be separated from the symmetry of the specific process, thus allowing one to calculate all dynamical parameters if the matrix elements of the photoionization and the Auger process as well as the angular momenta of the states involved are known. It is presumed that both processes—the photoionization and the Auger process—take place successively and that one process is not influenced by the other, implying a factorization of all dynamical parameters (two-step model of Auger decay). The spin-polarization components of the Auger electrons are then expressed in the same terms as for photoelectrons [see Eqs. (1) and (2)] using the relations [8]

$$\begin{aligned} &A_{\text{Auger}} = \beta_1 \mathcal{A}_{10}, \quad \alpha_{\text{Auger}} = -\gamma_1 \mathcal{A}_{10}, \\ &\beta_{\text{Auger}} = -2\,\alpha_2 \mathcal{A}_{20}, \quad \xi_{\text{Auger}} = \xi_2 \mathcal{A}_{20}, \end{aligned} \tag{3}$$

where the anisotropy coefficients $\mathcal{A}_{K0}$ describe the alignment ($\mathcal{A}_{20}$) and the orientation ($\mathcal{A}_{10}$) of the photoion and the other parameters characterize the intrinsic properties of the Auger decay. For the occurrence of an orientation $\mathcal{A}_{10}$ of the photoion, however, it is necessary to use circularly polarized light for photoionization. In the case of the excitation of an electron from a $J = 1/2$ substate the ion may only possess an orientation but no alignment, implying $\beta_{\text{Auger}} = 0$ and $\xi_{\text{Auger}} = 0$ for the Auger electron. In this case, apart from the cross section only the dynamical parameters A_{Auger} and α_{Auger} contain information about the Auger process.

In the nonrelativistic approximation, when the spin-orbit interaction is neglected, the dynamical photoionization parameters are not independent, and for photoelectrons from a $p_{1/2}$ and $p_{3/2}$ subshell the common nonrelativistic relationships hold at the same kinetic ener-

gies. Under these conditions the photoionization process is determined by three parameters, namely, the amplitudes of the matrix elements of the outgoing s and d waves, D_s and D_d, and the phase difference $(\delta_s - \delta_d)$ between the outgoing partial photoelectron waves. Moreover, $A_{\rm photo}$, $\xi_{\rm photo}$, $\alpha_{\rm photo}$, and $\beta_{\rm photo}$ depend solely on the ratio D_s/D_d and $(\delta_s - \delta_d)$ [31]. Since the Auger-electron polarization is connected with the anisotropy of the photoion by the polarization transfer [see Eq. (3)], the parameters $A_{\rm Auger}$, $\alpha_{\rm Auger}$, and $\beta_{\rm Auger}$ depend on the ratio D_s/D_d of the photoelectron matrix elements if the same approximation as for the photoelectrons is used. The phase difference of the two outgoing partial photoelectron waves, however, does not influence the dynamical parameters of the Auger electron, since the orientation $\mathcal{A}_{10}$ and the alignment $\mathcal{A}_{20}$ of the photoion are phase independent. In general, the intrinsic Auger parameters β_1, γ_1, α_2, and ξ_2 contain amplitudes and phase differences [8]. For a $^1S_0$ final ionic state, however, all intrinsic parameters are purely geometrical quantities and can be simply calculated in a model-independent way. Therefore, in this case simple relations exist between the parameters determining the spin polarization of Auger electrons as well as correlations between parameters of photoelectrons and Auger electrons, if only the two-step model is valid:

$$\begin{aligned} \xi_{\rm Auger}(1/2) = \xi_{\rm Auger}(3/2) &= 0, \\ \beta_{\rm Auger}(1/2) &= 0\,, \\ \alpha_{\rm Auger}(1/2) &= 4\,A_{\rm Auger}(1/2), \\ \alpha_{\rm Auger}(3/2) &= \frac{2}{5}\,A_{\rm Auger}(3/2), \\ A_{\rm photo}(1/2) &= -3\,A_{\rm Auger}(1/2). \end{aligned} \tag{4}$$

If, moreover, the spin-orbit interaction in the continuum is neglected [32] the following additional relationships hold:

$$\begin{aligned} A_{\rm Auger}(3/2) &= -\frac{5}{2}A_{\rm Auger}(1/2), \\ \beta_{\rm Auger}(3/2) &= \frac{2}{5} + \frac{18}{25}A_{\rm Auger}(3/2), \\ A_{\rm photo}(3/2) &= -\frac{3}{5}\,A_{\rm Auger}(3/2)\,. \end{aligned} \tag{5}$$

The calculations of the D_s and D_d dipole amplitudes for the $5p \rightarrow \epsilon s$ and $5p \rightarrow \epsilon d$ transitions have been performed within the HF approach and the nonrelativistic RPAE [33]. The RPAE uses the set of HF wave functions as a basis to take into account the intra- and intershell many-electron correlations. It is known that the latter plays a significant role in the photoionization processes for many-electron atoms. The integral equation for the RPAE dipole amplitudes D_i can be written in the following way [33]:

$$D_i(\omega) = d_i + \int \sum D(\epsilon)\frac{1}{\omega - \epsilon}U(\epsilon)d\epsilon + \mathcal{T}, \tag{6}$$

where d_i and D_i are the HF and RPAE amplitudes for transitions to state i, respectively, ϵ is the energy of the intermediate state, U is the combined Coulomb matrix element, and $\mathcal{T}$ denotes the time reversal of the first and second terms. The integration (summation) is performed over all excited intermediate states of the continuous and discrete spectrum. If the sum includes only one subshell from which the transition occurs, this is equivalent to intrashell correlations. Intershell interactions are taken into account in the case of two or more subshells included in the sum. In contrast to previous calculations for Ba atoms [21, 23, 33], we have now calculated the dipole matrix elements within the RPAE by including explicitly the interaction between $6s$, $5p$, $5s$, and $4d$ electrons (six dipole channels). The influence of the $6s$ outer subshell on the transition from the $5p$ subshell is rather small and may be neglected for D_s and D_d amplitudes. In comparison with the HF amplitudes the strongest changes for the transition amplitudes are caused by the intrashell correlation and the influence of the $4d$ subshell. The phase shifts δ_s and δ_d are obtained by the calculations of the HF continuum wave functions [33]. From the calculated dipole amplitudes the alignment and orientation tensors were determined according to the equations of Kabachnik and Lee [8] as well as the photoelectron and the Auger-electron polarization parameters.

IV. INTENSITY MEASUREMENTS

In Fig. 1 an electron kinetic energy spectrum obtained at $h\nu = 28.5$ eV and $\theta_{\rm mag}$ is shown. This spectrum is background corrected and normalized to the electron current in the storage ring. The spectrometer transmission was also taken into account by measurements of the Xe $5p$ photoionization using the known Xe $5p$ cross section [34].

Four main peaks occur: at $E_{\rm kin} = 9.5$ eV the $5p_{1/2}^{-1}$-$6s^{-2}$ Auger line with the corresponding photoline at $E_{\rm kin} = 3.8$ eV, and at $E_{\rm kin} = 7.5$ eV the $5p_{3/2}^{-1}$-$6s^{-2}$ Auger line with the corresponding photoline at $E_{\rm kin} = 5.8$ eV. The peak at $E_{\rm kin} = 7.5$ eV with its corresponding photopeak denoted by $^2P_{3/2}$ consists actually of two excitation and decay modes, assigned as [16]

$5p^5 5d(^1D)6s^2 D_{3/2} \rightarrow 5p^6\,^1S_0 + e^-_{\rm Auger}$, $E_{\rm kin} = 7.47$eV,

$5p^5 6s^2\,^2P_{3/2} \rightarrow 5p^6\,^1S_0 + e^-_{\rm Auger}$, $E_{\rm kin} = 7.57$eV.

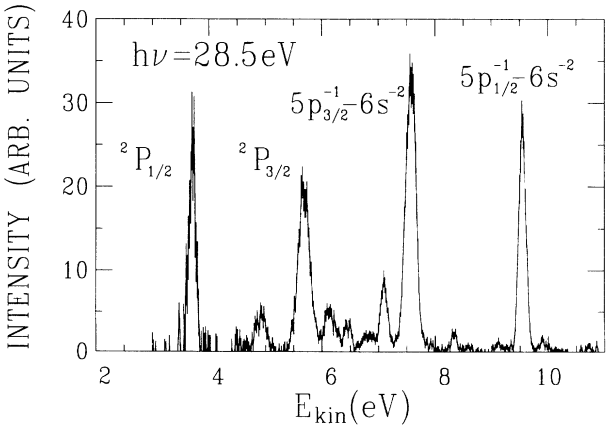

FIG. 1. Electron kinetic energy spectrum, obtained at $h\nu = 28.5$ eV, showing the two $5p_{1/2,\,3/2}^{-1}$-$6s^{-2}$ Auger lines and the corresponding photopeaks.

The line at $E_{\rm kin} = 7.47$ eV can be interpreted as a satellite of the $5p_{3/2}^{-1}$-$6s^{-2}$ Auger decay. In high resolution electron impact spectra [15,16] it was observed that both Auger lines are intense and calculations by Rose *et al.* [35] reveal that they both share the $5p^5 6s^2\,{}^2P_{3/2}$ character. This is due to the lowering of the $5d$ orbital in Ba^+, leading to strong $5d$-$6s$ mixing [16,35]. The influence of the additional line can be seen by the increased widths of both the Auger and the photopeak, $\Delta E_{\rm Auger} \simeq 220$ meV and $\Delta E_{\rm photo} \simeq 260$ meV, respectively, in comparison to the other spin-orbit component, the $5p_{1/2}^{-1}$-$6s^{-2}$ Auger line with $\Delta E_{\rm Auger} \simeq 130$ meV. According to the calculations [35] the transition from the $Ba^+\,{}^2P_{1/2}$ state is much less affected by configuration interaction with almost 80% $5p^5\,6s^2$ character. The photolines possess a slightly larger width due to the monochromator resolution $\Delta\lambda = 0.18$ nm, which does not influence the peak width of the Auger-electron intensity but leads to a broadening of the photoelectron lines with $\Delta E_{\rm kin} \simeq 120$ meV. Beside these major features, several lines with smaller intensities appear. They are satellites with mainly $J = 3/2$ character, giving rise to a deviation from the nonrelativistic ratio of $\sigma_{1/2}/\sigma_{3/2} = 0.5$ to $\sigma_{1/2}/\sigma_{3/2} \simeq 1$ for the $5p^{-1}$-$6s^{-2}$ main lines. This intensity borrowing effect was also observed in $2p$ photoionization of magnesium, where the occurrence of satellite peaks is accounted for by a spectroscopic factor, lowering the amplitudes of the matrix elements but leaving the ratio D_s/D_d unchanged [36].

In Fig. 2 the measured dependence of the Auger-electron intensity on the photon energy is shown for $5p_{1/2}^{-1}$-$6s^{-2}$ and $5p_{3/2}^{-1}$-$6s^{-2}$ transitions, respectively. For both data sets the spectrometer was held fixed at the kinetic energy of the Auger electrons and the monochromator was scanned. The spectra were normalized to the electron current in the storage ring and to the transmission characteristics of the monochromator determined with a calibrated photodiode. The two data sets are placed on a common intensity scale as determined from the ratio of the peak intensities of the $5p_{1/2}^{-1}$-$6s^{-2}$ and the $5p_{3/2}^{-1}$-$6s^{-2}$ Auger lines of several electron kinetic energy spectra at different photon energies. Both spectra consist

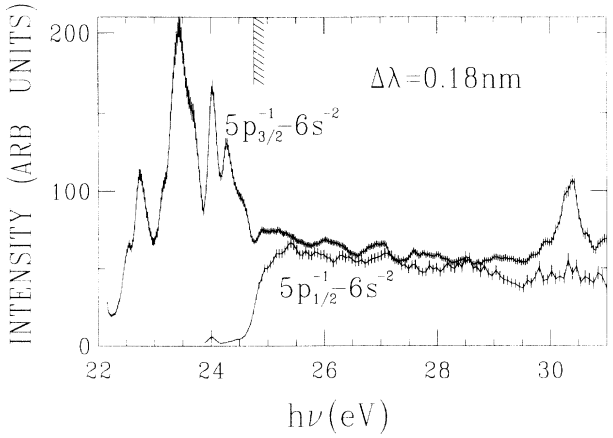

FIG. 2. Energy dependence of the Auger electron intensity for both $5p^{-1}$-$6s^{-2}$ Auger lines.

of the average of at least 5 scans, so that small variations in the atomic beam intensity are averaged. Below the threshold of the $5p_{1/2}^{-1}$-$6s^{-2}$ Auger decay at 24.75 eV a pronounced resonance structure occurs in the $5p_{3/2}^{-1}$-$6s^{-2}$ spectrum, which is caused by spin-orbit autoionization of the excited barium atom. The main features are also present in the total absorption spectrum [12,13] for the same energy range. This is reasonable, since subsequent $O_{2,3}$-P_1P_1 Auger-electron emission after photoexcitation is the dominant decay mode of these highly excited states. The pronounced intensity maximum between 23 eV and 24 eV is due to an overlap of several members of the Rydberg series, mainly $\rightarrow 5p^5\,6s^2\,({}^2P_{1/2})\,6d$, and higher members of the c series, following the notation of Connerade *et al.* [12]. The shoulder in the high energy side of the peak is caused by the third members of the b series, which have the tentative assignment by Connerade *et al.* $[\rightarrow 5p^5\,6s^2\,({}^2P_{1/2})\,9s]$ and $[\rightarrow 5p^5\,5d^2\,({}^2P_{1/2})\,9s]$. The line at 24 eV is mainly due to the transition $[\rightarrow 5p^5\,6s^2\,({}^2P_{1/2})\,7d]$ and finally the peak at 24.3 eV is caused by $[\rightarrow 5p^5\,6s^2\,({}^2P_{1/2})\,8d]$. Furthermore, beyond the threshold for $5p_{1/2}^{-1}$-$6s^{-2}$ between 25 eV and 28 eV a very weak resonance structure is superimposed on the much stronger contribution originating from direct ionization. This weak feature is also present in the previously measured absorption spectra [12]. The intensity maximum in the $5p_{3/2}^{-1}$-$6s^{-2}$ Auger spectrum at 30.4 eV is caused by photoelectrons which have the same kinetic energy as the Auger electrons at this photon energy.

V. SPIN-POLARIZATION MEASUREMENTS AND CALCULATED RESULTS

At $h\nu = 25.8$ eV the angular distributions of the spin polarization components $A(\theta)$ [9] and $P_\perp(\theta)$ for the $5p_{1/2}^{-1}$-$6s^{-2}$ Auger channel were measured (Fig. 3). For the experimental $P_\perp(\theta)$ distribution the apparatus related asymmetry is eliminated by measurements at both $+\theta$ and $-\theta$. The component $P_\perp(\theta)$ is expected to vanish at all angles, since we consider a single channel Auger decay, and dynamical polarization can only occur as a consequence of the interference of at least two outgoing partial waves. The measured $P_\perp(\theta)$ distribution is in good agreement with this requirement. Moreover, for an intermediate photoion state with total angular momentum $J \leq 1/2$ the alignment parameter $\mathcal{A}_{20}$ vanishes, leading to an isotropic angular intensity distribution ($\beta_{\rm Auger} = 0$). This was assumed in the least-squares fit procedure to the experimental data, improving the accuracy of the fitted dynamical parameters $A_{\rm Auger}$ and $\alpha_{\rm Auger}$, due to the reduction of the number of free fit parameters. The experimental ratio $\frac{\alpha_{\rm Auger}}{A_{\rm Auger}} = 4.2 \pm 1.0$ is in good agreement with the expected value of $\frac{\alpha_{\rm Auger}}{A_{\rm Auger}} = 4.0$ [see Eq. (4)], which follows for a $5p_{1/2}^{-1}$-$6s^{-2}$ Auger decay from symmetry considerations. At $h\nu = 23.5$ eV for the $5p_{3/2}^{-1}$-$6s^{-2}$ Auger process a ratio $\frac{\alpha_{\rm Auger}}{A_{\rm Auger}} = 0.6 \pm 0.3$ was extracted from the angular distribution [9], while $\frac{\alpha_{\rm Auger}}{A_{\rm Auger}} = 0.4$ is expected from theory. Both ratios $\frac{\alpha_{\rm Auger}}{A_{\rm Auger}}$

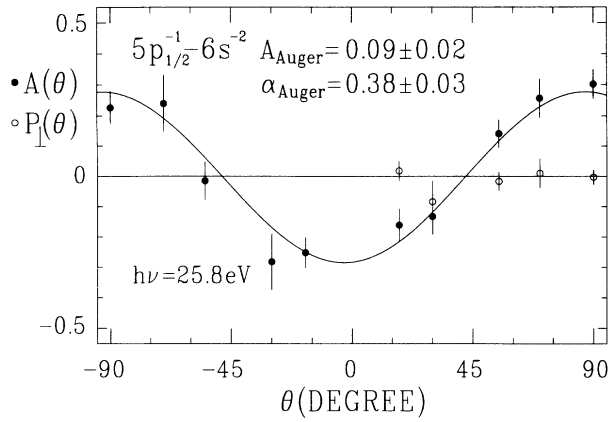

FIG. 3. Angular distribution of the spin-polarization component $A(\theta)$, •, and $P_\perp(\theta)$, ○, for the $5p_{1/2}^{-1}$-$6s^{-2}$ Auger line at a photon energy of $h\nu = 25.8$ eV. The solid line represents a least-squares fit to the data according to Eq. (1).

do not depend on the photon energy even in a relativistic treatment and if a deviation existed it could only be caused by a breakdown of the two-step model.

The measured values for A_{Auger} obtained at different photon energies for $O_{2,3}$-P_1P_1 Auger electrons are shown in Fig. 4. The absolute value of the integral spin polarization A_{Auger} resulting from the $5p_{1/2}^{-1}$-$6s^{-2}$ Auger decay is lower than for $5p_{3/2}^{-1}$-$6s^{-2}$, in accordance with the nonrelativistic approximation. In the case of a $5p_{1/2}^{-1}$-$6s^{-2}$ Auger decay the range of possible values for A_{Auger} varies only between $-\frac{1}{3}$ and $\frac{1}{6}$ while for the $5p_{3/2}^{-1}$-$6s^{-2}$ Auger decay A_{Auger} can take on values from $-\frac{5}{12}$ to $\frac{10}{12}$. In the case of a $^1S_0$ final ionic state the parameter A_{Auger} is a direct measure for the degree of orientation of the photoion as was discussed in detail previously [9]. The orientation coefficients $\mathcal{A}_{10}(1/2)$ and $\mathcal{A}_{10}(3/2)$ may be obtained by multiplication of the values of $A_{\text{Auger}}(1/2)$ and $A_{\text{Auger}}(3/2)$ in Fig. 4 by a factor of -3 and $3/\sqrt{5}$, respectively, resulting in orientation coefficients on the order of -0.3 for both spin-orbit states in the free continuum region. The A_{Auger} values at $h\nu = 25.8$ eV for the $5p_{1/2}^{-1}$-$6s^{-2}$ and at $h\nu = 23.5$ eV for the $5p_{3/2}^{-1}$-$6s^{-2}$ Auger decay have a lower statistical error, since they were extracted from a fit procedure to the angular distributions of the spin polarization component $A(\theta)$ (Fig. 3), whereas the other A_{Auger} values are derived from measurements at $\theta_{\text{mag}} = \pm 54.7°$, where $A(\theta_{\text{mag}}) = \gamma A_{\text{Auger}}$ holds. The parameter A_{Auger} for the $5p_{1/2}^{-1}$-$6s^{-2}$ Auger decay shows hardly a variation with photon energy in contrast to the $5p_{3/2}^{-1}$-$6s^{-2}$ electrons, which have a more pronounced energy dependence. For this behavior, on the one hand, the larger scaling of the parameter $A_{\text{Auger}}(3/2)$ $[A_{\text{Auger}}(3/2) = -2.5A_{\text{Auger}}(1/2)]$ is responsible and, on the other hand, the appearance of resonances below the threshold for the $5p_{1/2}^{-1}$-$6s^{-2}$ Auger decay is the cause. According to Connerade *et al.* [12] these resonances at $h\nu = 23.5$ eV and at $h\nu = 24.1$ eV have mainly d character. This explains the larger negative values of A_{Auger} in comparison to the values for the continuum where direct ionization dominates. The experimental values are compared with results of theoretical calculations using the Hartree-Fock and the RPAE approaches. For the $5p_{1/2}^{-1}$-$6s^{-2}$ Auger parameter A_{Auger} both theories are in agreement with the experimental data, with the exception of the most precisely determined data point at $h\nu = 25.8$ eV, where only the RPAE approach coincides with the experimental result. For the $5p_{3/2}^{-1}$-$6s^{-2}$ Auger decay in the autoionization region a direct comparison with the theory is not possible due to the presence of the resonances which are not taken into account in the calculation. The influence of the $5p^5\,5d^2\,(^2P_{1/2})\,nd\ ^1P_1$ resonances [12] should give rise to an increase of the D_d amplitude for the two values (n=6,7) measured in this region. This explains the corresponding large negative values of A_{Auger}. Incidentally they lie close to the HF calculation, which predicts a lower ratio $|D_s/D_d|^2$ than the RPAE. Beyond the $5p_{1/2}^{-1}$-$6s^{-2}$ threshold, however, again the RPAE is in better agreement, although the nonresolved Auger satellite line also contributes to the parameter A_{Auger} for the $5p_{3/2}^{-1}$-$6s^{-2}$ line. For the parameter α_{Auger} (Fig. 5) the conditions are reversed, since

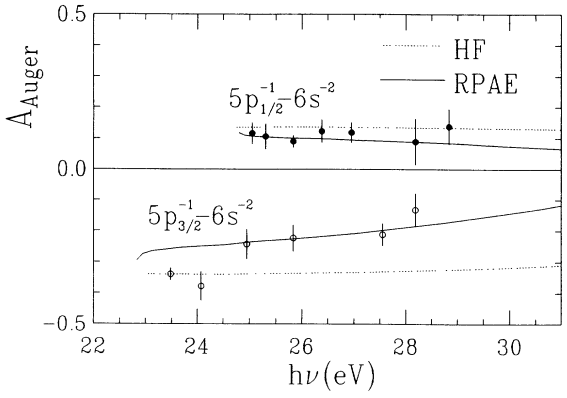

FIG. 4. Energy dependence of the calculated spin-polarization parameter A_{Auger} for the $5p_{1/2,\,3/2}^{-1}$-$6s^{-2}$ Auger lines in comparison with experimental data. Below and above $h\nu = 25$ eV the spectral resolution was $\Delta\lambda = 0.18$ nm and $\Delta\lambda = 0.36$ nm, respectively.

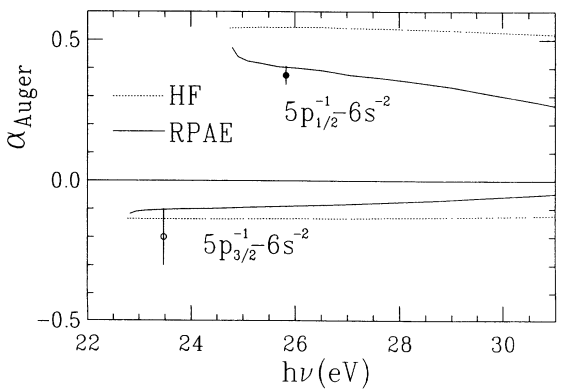

FIG. 5. Spin-polarization parameters α_{Auger} for both Auger decay channels in HF and RPAE calculations in comparison with the measured values extracted from the angular distribution of the spin-polarization component $A(\theta)$.

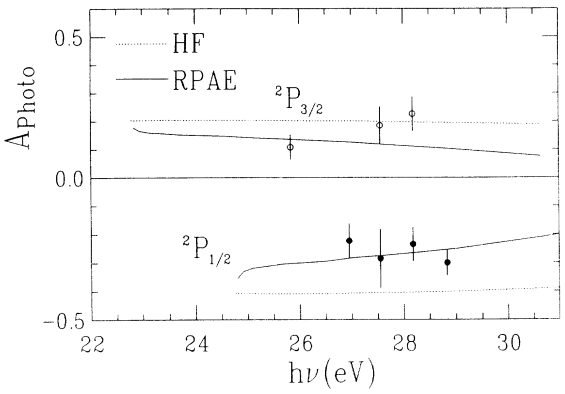

FIG. 6. Measured and calculated spin-polarization parameters A_{photo} for photoelectrons corresponding to photoions in the $^2P_{1/2}$ and $^2P_{3/2}$ states.

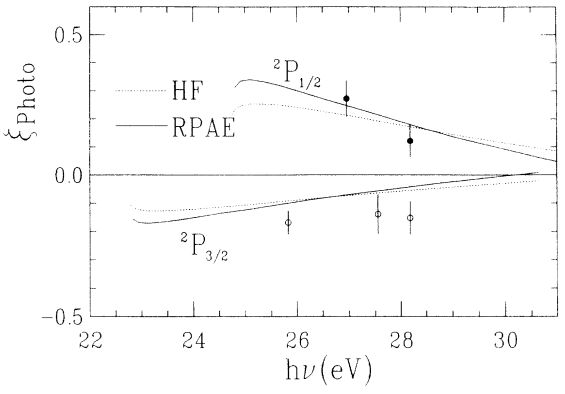

FIG. 7. Measured and calculated spin-polarization parameter ξ_{photo} for photoelectrons corresponding to photoions in the $^2P_{1/2}$ and $^2P_{3/2}$ states.

the allowed values for $\alpha_{\text{Auger}}(3/2)$ range from $-\frac{1}{6}$ to $\frac{1}{3}$ in the nonrelativistic approach, while for $\alpha_{\text{Auger}}(1/2)$ they can go from $-\frac{4}{3}$ to $\frac{2}{3}$. Hence the difference between the HF and the RPAE approach is larger for the $\alpha_{\text{Auger}}(1/2)$ value and the test of the theory is more stringent in that case. The value for $\alpha_{\text{Auger}}(3/2)$, however, is compatible with both calculated values within the experimental error and again reflects the influence of an increased d-wave contribution for the outgoing photoelectron in the resonance region.

It was not always possible to measure the spin polarization of the photoelectrons at the corresponding energy where the Auger-electron spin polarization was observed, since the buildup of contact potentials diminished the transmitted photoelectron intensity at low kinetic energies. The experimental data and the theoretical curves for the photoelectron spin-polarization parameter A_{photo} are displayed in Fig. 6. Fair agreement is obtained, in particular with respect to the Ba^+ $^2P_{1/2}$ final ionic state, where the measured data coincide with the RPAE approach. In addition to Figs. 4 and 6, in Table I the experimental data are listed in a comparison of the spin-polarization parameters A of the Auger and the photoelectrons. This cross comparison has been discussed in detail elsewhere [37], but the list of the measured values available is now more extensive and therefore given in the table for completeness. The ratio $\frac{A_{\text{Auger}}(1/2)}{A_{\text{photo}}(1/2)}$ can serve as a direct check of the validity of the two-step model. The parameters A_{Auger} calculated from the photoelectron spin polarization according to Eq. (4) are in good agreement with the measured value A_{Auger}. Only at $h\nu = 26.95$ eV the calculated and the measured Auger parameters differ slightly. For the $5p_{3/2}^{-1}$-$6s^{-2}$ Auger decay [37] the ratio might be influenced by relativistic effects and the deviations between $-5/3\,A_{\text{photo}}$ and A_{Auger} confirm this assumption. At $h\nu = 28.18$ eV the parameter A_{photo} is even larger than the corresponding A_{Auger} value. The only measured parameter which contains information about the phase difference between the outgoing s and d waves of the photoelectron is the parameter ξ_{photo} (Fig. 7). In the photon energy range observed here both calculations give similar results for ξ_{photo}, and for the $^2P_{1/2}$ ion ξ_{photo} is in agreement with both the HF and the RPAE theory. For the creation of the $^2P_{3/2}$ hole state via photoionization, however, both approaches deviate slightly from the measured dynamical polarization ξ_{photo}. The absolute value of $\xi_{\text{photo}}(3/2)$ is larger than expected from the nonrelativistic approach.

VI. CONCLUSIONS

The energy dependences of the $O_{2,3}$-P_1P_1 Auger-electron doublet emitted after the creation of a $5p^{-1}$ hole state of Ba^+ as well as of the corresponding $5p$ photoelectrons have been examined both experimentally and theoretically with respect to the spin polarization. The measurements of the Auger-electron yield showed that the influence of resonant contributions is large below and small above the threshold for $5p_{1/2}^{-1}$-$6s^{-2}$ Auger-electron emission. Apart from the variation due to the increased ϵd photoelectron transition amplitudes in the resonances, the polarization parameters A_{Auger} display

TABLE I. Comparison of the spin-polarization components A_{photo} and A_{Auger} and the value A_{Auger} calculated from A_{photo} according to Eq. (4) for the $J = 1/2$ and $J = 3/2$ channels.

$h\nu$ (eV)	25.83	26.95	27.55	28.18	28.83
$A_{\text{photo}}(1/2)$		-0.22 ± 0.06	-0.29 ± 0.10	-0.24 ± 0.06	-0.30 ± 0.05
$A_{\text{Auger}}(1/2)$	0.09 ± 0.02	0.12 ± 0.03	–	0.09 ± 0.07	0.14 ± 0.06
$-1/3\,A_{\text{photo}}(1/2)$		0.07 ± 0.02	0.10 ± 0.03	0.08 ± 0.02	0.10 ± 0.02
$A_{\text{photo}}(3/2)$	0.11 ± 0.04		0.19 ± 0.07	0.23 ± 0.06	
$A_{\text{Auger}}(3/2)$	-0.22 ± 0.04		-0.21 ± 0.04	-0.13 ± 0.05	
$-5/3\,A_{\text{photo}}(3/2)$	-0.18 ± 0.07		-0.32 ± 0.12	-0.38 ± 0.09	

only a weak dependence on the photon energy in the region studied. The experimental results confirm the validity of the relationships between the various dynamical parameters as far as they could be tested. Within the two-step model of Auger decay the parameter A_{Auger} is directly connected with the photoelectron polarization parameter A_{photo} via the photoion polarization $\mathcal{A}_{10}$. In particular, for the single-channel Auger transition examined here, the parameters A_{Auger}, $\mathcal{A}_{10}$, and A_{photo} are proportional to each other for the $5p_{1/2}$ case, and also for the $5p_{3/2}$ ionization within the LS approximation. For the $J = 1/2$ case, the experimental data were found to be in agreement with the relationships connecting the Auger-electron and the photoelectron emission process.

With respect to the comparison of the experimental data with the theoretical calculations, better agreement was found with the RPAE theory than with the HF approach; in particular, the RPAE describes well all dynamical parameters examined which are related to the $5p_{1/2}$ ionization. In the case of the $5p_{3/2}$-$6s^{-2}$ Auger decay there are some small deviations between the experiment and the RPAE calculation which can be explained by the presence of resonant excitation and the composition of the observed Auger and photoline of two transitions. Another possible reason is the neglection of the spin-orbit splitting of the outgoing d waves. While this does not affect $5p_{1/2}^{-1}$ ionization since only the $d_{3/2}$ component contributes, for $5p_{3/2}^{-1}$ ionization both $d_{3/2}$ and $d_{5/2}$ components are important and the relative phase between them. Therefore, the $5p_{3/2}$ channel can be expected to be influenced by relativistic effects. Finally, in the theoretical calculations we completely ignore rearrangement effects which can, in principle, change the ratio of the partial amplitudes D_s/D_d and thus the dynamical parameters governing the polarization. In the future it will be of interest to perform spin-polarization studies in more complicated cases where the final states do not have closed shells and several Auger channels occur or where spectator electrons are present.

ACKNOWLEDGMENTS

Support by the BESSY staff and the assistance of G. Snell is gratefully acknowledged. N.M.K. is grateful to the Fritz-Haber Institut der Max-Planck-Gesellschaft and the University of Bielefeld (SFB 216 of DFG) for hospitality and financial support. This work was funded by the BMFT (055PBAXI3).

[1] W. Mehlhorn, in *X-Ray and Atomic Inner-Shell Physics*, Proceedings of the International Conference on X-ray and Atomic Inner-Shell, Physics, edited by B. Crasemann, AIP Conf. Proc. No. 94 (AIP, New York, 1982), p. 55.
[2] W. Mehlhorn, in *Atomic Inner-Shell Physics*, edited by B. Crasemann (Plenum, New York, 1985), p. 199.
[3] H. Klar, J. Phys. B **13**, 4741 (1980).
[4] N. M Kabachnik J. Phys. B **14**, L377 (1981).
[5] U. Hahn, J. Semke, H. Merz, and J. Kessler, J. Phys. B **18**, 417 (1985).
[6] H. Merz and J. Semke, in *X-Ray and Inner-Shell Processes, Knoxville, 1990*, Proceedings of the Fifteenth International Conference on X-ray and Inner-Shell Processes, edited by T. A. Carlson, M. O. Krause, and S. T. Manson, AIP Conf. Proc. No. **215** (AIP, New York 1990), p. 719.
[7] T. A. Carlson, D. R. Mullins, C. E. Beall, B. W. Yates, J. W. Taylor D. W. Lindle, and F. A. Grimm, Phys. Rev. A **39**, 1170 (1989).
[8] N. M. Kabachnik and O. V. Lee, J. Phys. B **22**, 2705 (1989).
[9] R. Kuntze, M. Salzmann, N. Böwering, and U. Heinzmann, Phys. Rev. Lett. **70**, 3716 (1993).
[10] P. Stoppmanns, B. Schmiedeskamp, B. Vogt, N. Müller, and U. Heinzmann, Phys. Scr. **T41**, 190 (1992).
[11] D. M. P. Holland and K. Codling, J. Phys. B **13**, L293 (1980).
[12] J. P. Connerade, M. W. D. Mansfield, G. H. Newsom, D. H. Tracy, and M. A. Baig, Philos. Trans. R. Soc. London Ser. A **290**, 327 (1979).
[13] M. A. Baig, J. P. Connerade, C. Mayhew, and K. Sommer, J. Phys. B **17**, 371 (1984).
[14] R. A. Roig, J. Opt. Soc. Am. **66**, 1400 (1976).
[15] W. Mehlhorn, B. Breuckmann, and D. Hausamann, Phys. Scr. **16**, 177 (1977).
[16] D. Rassi and K. J. Ross, J. Phys. B **13**, 4683 (1980).
[17] H. Hotop and D. Mahr, J. Phys. B **8**, L301 (1975).
[18] P. H. Kobrin *et al.*, J. Phys. B **16**, 4339 (1983).
[19] R. A. Rosenberg, M. G. White, G. Thornton, and D. A. Shirley, Phys. Rev. Lett. **43**, 1384 (1979).
[20] J. M. Bizau, D. Cubaynes, P. Gerard, and F. J. Wuilleumier, Phys. Rev. A **40**, 3002 (1989).
[21] G. Wendin, in *Proceedings of the IVth International Conference on Vacuum Ultraviolet Radiation Physics, Hamburg, 1974*, edited by E. Koch, R. Haensel, and C. Kunz (Vieweg-Pergamon, Braunschweig, 1974), p. 225.
[22] E. G. Berezhko, N. M. Kabachnik, and V. S. Rostovsky, J. Phys. B **11**, 1749 (1978).
[23] E. G. Berezhko, V. K. Ivanov, and N. M. Kabachnik, Phys. Lett. **66A**, 474 (1978).
[24] U. Hergenhahn, N. M. Kabachnik, and B. Lohmann, J. Phys. B **24**, 4759 (1991).
[25] B. Lohmann, U. Hergenhahn, and N. M. Kabachnik, J. Phys. B **26**, 3327 (1993).
[26] B. Lohmann, J. Phys. B **25**, 4163 (1992).
[27] F. Schäfers, W. Peatman, A. Eyers, Ch. Heckenkamp, G. Schönhense, and U. Heinzmann, Rev. Sci. Instrum. **57**, 1032 (1986).
[28] K. Jost, J. Phys. E **12**, 1006 (1979).
[29] Ch. Heckenkamp, A. Eyers, F. Schäfers, G. Schönhense, and U. Heinzmann, Nucl. Instrum. Methods A **246**, 500 (1986).
[30] Ch. Heckenkamp, F. Schäfers, G. Schönhense, and U. Heinzmann, Phys. Rev. Lett. **52**, 421 (1984).
[31] N. A. Cherepkov, J. Phys. B **12**, 1279 (1979).
[32] W. Bußert and H. Klar, Z. Phys. A **312**, 315 (1983).
[33] M. Ya. Amusia and N. A. Cherepkov, Case Stud. At. Phys. **5**, 47 (1975).
[34] J. B. West and J. Morton, At. Data Nucl. Data Tables **22**, 103 (1975).
[35] S. J. Rose, I. P. Grant, and J. P. Connerade, Philos. Trans. R. Soc. London **296**, 527 (1980).
[36] B. Kämmerling, A. Hausmann, J. Läuger, and V. Schmidt, J. Phys. B **25**, 4773 (1992).
[37] R. Kuntze, M. Salzmann, N. Böwering, and U. Heinzmann, Z. Phys. D (to be published).